I&EC research
Industrial & Engineering Chemistry Research

pubs.acs.org/IECR

Article

NiGa Unsupported Catalyst for CO_2 Hydrogenation at Atmospheric Pressure. Tentative Reaction Pathways

Marina Cortés-Reyes, Ibrahim Azaoum, Sergio Molina-Ramírez, Concepción Herrera, M. Ángeles Larrubia, and Luis J. Alemany*

Cite This: *Ind. Eng. Chem. Res.* 2021, 60, 18891−18899

Read Online

ACCESS | Metrics & More | Article Recommendations | Supporting Information

ABSTRACT: The hydrogenation of CO_2 is presented as a catalytic strategy for CO_2 utilization and an approach to the development of sustainable processes to obtain products with high added value, such as CO, CH_4, and CH_3OH. An unsupported Ni_xGa_y model catalyst with high surface area was synthesized by an ultrasonic-assisted coprecipitation method. The in situ H_2-treatment and the activation temperature (600, 700, and 800 °C) are key in the phases present in the catalyst and, therefore, in the reactivity in the CO_2 hydrogenation reaction at atmospheric pressure. Operating conditions have been selected that maximize the selectivity to be able to correlate phases, surface, and reactivity. Independently of the H_2/CO_2 feed ratio, after treatment in hydrogen at 600 °C, CO selectivity values are higher than 97%, via a reverse water gas shift reaction, with $Ni_{13}Ga_9$ and Ni metallic being the main phases detected. The H_2-treatment at 700 °C increases the proportion of Ni^0 and $Ni_{13}Ga_9$ phases, and even with the use of a H_2/CO_2 feeding ratio of 3, methanation is the only reaction that occurs. At 800 °C, Ni_5Ga_3 is the main phase detected, and methanol is formed at 150 °C, through the intervention of a necessary formate species; when the reaction temperature is higher than 400 °C, the rWGS is the only observable reaction, with complete CO formation.

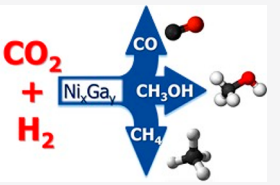

1. INTRODUCTION

The continuous increase in greenhouse gases (GHG) emissions into the atmosphere is producing an increase in the global average temperature (global warming).[1−3] This premise makes it necessary to search for technologies that allow reducing the emission of these pollutants or avoiding their production, such as the investment in low-carbon energy sources.[4] To date, it has been difficult to modify all the sources and ways of producing energy in the industrial sector,[5] and the emissions of CO_2, which is the main GHG,[6] will continue to be high in the short term. Thus, the development of new advanced technologies for the elimination of CO_2 is required to reduce its concentration in the atmosphere and the negative impact on the environment.

Although there are potential techniques, such as carbon capture and storage or utilization (CCS or CCU),[7−9] that could be used to reduce the anthropogenic carbon dioxide emissions, CO_2 hydrogenation, especially if green H_2 is used, is a promising strategy to recycle CO_2 and obtain value-added products, mainly methanol, methane, or carbon monoxide.[10−12] Because CO_2 is inert under normal conditions,[13,14] the transformation by reduction with hydrogen usually requires high pressures or temperatures, so catalysts are needed and new mechanisms are being investigated to work at atmospheric pressure. The main reactions that could take place are expressed in eqs 1−3 and the products are intermediates with which a great variety of products highly demanded in the chemical industry can be produced.[15−19]

$$CO_2(g) + H_2(g) \leftrightarrows CO(g) + H_2O(g) \quad \Delta H = 41.2\ kJ\cdot mol^{-1} \tag{1}$$

$$CO_2(g) + 3H_2(g) \leftrightarrows CH_3OH(g) + H_2O(g) \quad \Delta H = -49.5\ kJ\cdot mol^{-1} \tag{2}$$

$$CO_2(g) + 4H_2(g) \leftrightarrows CH_4(g) + 2H_2O(g) \quad \Delta H = -165\ kJ\cdot mol^{-1} \tag{3}$$

The understanding of the CO_2 hydrogenation process is crucial to develop potential breakthrough technologies at the industrial scale.[20] CO is obtained from the reverse water gas shift reaction (rWGS). High operation temperatures are usually required, ranging from 200 to 800 °C,[21] as it is thermodynamically favored. Catalysts used for these processes are metallic nanoparticles (mainly Pt and Cu) supported on oxides such as TiO_2, although it is necessary to add thermal stabilizers to avoid sintering of the nanoparticles at high temperatures.[22,23]

Special Issue: José Luis García Fierro Festschrift

Received: August 3, 2021
Revised: October 25, 2021
Accepted: October 25, 2021
Published: December 6, 2021

On the other hand, CO_2 hydrogenation to methanol has attracted increasing attention in recent years[24] since methanol has many applications, as it can be used as a raw material in the production of other products or even as an alternative fuel. Low temperature and high pressures are necessary due to the exothermic nature of the reaction, thus requiring the use of catalysts to carry out the process, such as Pd/ZnO, which presents some activity for hydrogenation to methanol and for low pressure, at 4.5 bar.[25] Besides, Cu−Zn supported on Al_2O_3 or ZrO_2 are the commercial catalysts although their low catalytic activity and poor stability are reported.[26] The modification with In, Ce, or Ti and the substitution by other materials, such as Ni−Ga, are presented as promising catalytic technologies to overcome the disadvantages of current catalysts;[27−30] however, obtaining high conversions and high selectivity values to methanol at atmospheric pressure is still a challenge.

Hydrogenation of CO_2 can also produce methane via the Sabatier reaction (eq 3). Methanation is an exothermic reaction, thermodynamically favored at relatively low reaction temperature (25−400 °C), so it has high kinetic limitations and requires suitable catalysts such as Pd, Ru, Ni, Rh, or Co.[31−34] Nevertheless, the reaction mechanism and the species that are involved in the process are still under investigation and could help to develop active catalysts. To decrease the energy consumption demand and increase the process safety, catalytic technologies that operate at atmospheric pressure are recommended. Moreover, as described above, bimetallic catalysts, especially nickel-based catalysts,[34−36] are presented as economic catalysts with high activity in the transformation of CO_2 by reduction, and a more in-depth knowledge of this type of material is desired.

Therefore, this work is focused on the valorization of CO_2 by catalytic hydrogenation at atmospheric pressure to obtain high added-value products using a novel unsupported catalyst based on Ni (Ni−Ga). The reaction pathway will be established depending on the structural and surface characteristics and the product yield.

2. EXPERIMENTAL SECTION

2.1. Materials Preparation and Characterization. Ni−Ga bimetallic catalysts were synthesized by the coprecipitation method, using $Ni(NO_3)_2{\cdot}6H_2O$ and $Ga(NO_3)_3{\cdot}xH_2O$ supplied by Panreac and Acros, respectively, as precursors. The amount of the precursors was established to keep the Ni/Ga atomic ratio at 5:3, and nitrates were dissolved in distilled water under stirring. To increase the surface area of the unsupported catalyst, 3 wt % (wih respect to gallium and nickel oxides) of Ludox HS-40 colloidal silica (from Aldrich, 40 wt % SiO_2) was added, and the mixture was left under stirring overnight. The solution was sonicated in two pulses of 5 s with the Ultrasonic Processor UIP1000hd (Hielscher) using a titanium sonotrode with unchangeable frequency of 20 kHz and 300W·cm^{-2} of ultrasonic power intensity. Then, the pH was adjusted to 9 by the addition of ammonia solution (30%, Panreac), in order to ensure the precipitation of nickel and gallium hydroxyls. The solution was decanted for 24 h and the liquid phase was removed. The resulting solid product was washed several times with distilled water and dried at 100 °C overnight. The dried powder was calcined at 400 °C in air for 2 h (5 °C·min^{-1}) in a muffle furnace and the material obtained was denoted as fresh NiGa catalyst. NiGa catalyst was reduced at different temperatures from 600 to 800 °C in H_2 (20% in He) for 2 h, and the samples were labeled as NiGa_RT, where T is the temperature of the reduction.

X-ray diffraction (XRD) patterns between 5 and 80° of Bragg Angle (2θ) were recorded with an EMPYREAN diffractometer (PANanalytical) equipped with an automatic loader and a rotating sample holder under Cu Kα radiation (λ = 1.548 Å), with 45 kV and 40 mA. The specific surface area and pore volume were determined on a Micromeritics ASAP 2420 instrument by nitrogen adsorption−desorption isotherms performed at liquid nitrogen temperature (−196 °C). Before the analysis, the samples were outgassed in vacuum (1×10^{-3} Pa) for 5 h at 453 K. The BET (Brunauer−Emmett−Teller) and the *t*-plot methods were used to determine the specific surface area and the pore volume, respectively. Raman spectra were recorded from 100 to 2500 cm^{-1} in a DXR Raman microscope (Thermo Scientific), working at 532 nm, 10 mW, and 5 s of accumulation time and with a charge couple device (CCD) detector. The XPS spectra were obtained by a Physical Electronics 5700 spectrometer with a Mg Kα X-ray source and a hemispherical electron analyzer. The regions of C 1s, O 1s, Ni 2p, Ga $2p_{3/2}$, and Si 2p were analyzed. The C 1s peak at 284.8 eV was used as an internal standard for determining peak positions, with ±0.2 eV accuracy. All deconvolutions of experimental curves were done with Gaussian−Lorentzian line fitting, minimizing the (χ^2) chi-square values.

2.2. Catalytic Activity. The activity of the catalyst in the hydrogenation of CO_2 was evaluated in a tubular fixed-bed stainless steel reactor (i.d., 9 mm; length, 15 cm) equipped with a coaxial thermocouple placed at the center of the catalytic bed. An online chromatograph (Agilent 7820A GC) equipped with a thermal conductivity detector (TCD) and flame ionization detector (FID) was used to quantify the gas composition. Prior to the CO_2 hydrogenation reaction test, the catalyst was activated in situ with H_2 (20% H_2/He) for 2 h. Experiments were carried out at atmospheric pressure in the temperature range between 150 and 500 °C, using 0.1 g of catalyst (100−125 μm) and 50 cm^3·min^{-1} (gas hourly space velocity (GHSV) = 10^4 h^{-1}). The concentration of CO_2 was kept at 5% in volume, the hydrogen concentration was varied (5−20%) to obtain H_2/CO_2 ratio values from 1 to 4, and helium was used as carrier.

The catalytic activity was measured in terms of CO_2 conversion and product distribution. The conversion of CO_2 (X_{CO2}) and the selectivity of the main products (CH_3OH, CO, CH_4) at the outlet stream were calculated using the following equations:

$$X_{CO_2} = \frac{F^0_{CO_2} - F_{CO_2}}{F^0_{CO_2}} 100 \tag{4}$$

$$S_i = \frac{F_i}{\Sigma F_i} 100 \tag{5}$$

where F_{CO2} is the outlet flow of CO_2 (mol·min^{-1}), F^0_{CO2} is the inlet flow of CO_2 (mol·min^{-1}), F_i is the flow of component '*i*' produced (mol·min^{-1}) and $\sum F_i$ (mol·min^{-1}) is the total flow of products in the outlet stream. The yield of each product of interest was obtained from multiplication of conversion and selectivity.

3. RESULTS AND DISCUSSION

3.1. Material Characterization. NiGa catalyst was synthesized by the coprecipitation of the precursors, adding

https://doi.org/10.1021/acs.iecr.1c03115
Ind. Eng. Chem. Res. 2021, 60, 18891−18899

colloidal silica as an area promoter. In Table 1, the textural properties of the fresh and reduced (at any temperature) NiGa catalyst are included. No significant modifications were detected in the BET area and pore volume when the catalyst was reduced at different temperatures, and the average values are included in the table.

Table 1. Textural Properties of NiGa Catalysts

	NiGa	NiGa_red
A_{BET} ($m^2 \cdot g^{-1}$)	177	34
V_p ($cm^3 \cdot g^{-1}$)	0.28	0.11

Values around 90 $m^2 \cdot g^{-1}$ were reported for NiGa alloys prepared by the coprecipitation method without reduction;[37] however, a value of 177 $m^2 \cdot g^{-1}$ was obtained for the synthesized sample. This value indicates the beneficial effect of incorporating 3 wt % of colloidal silica during the synthesis process which serves as a seed to generate a homogeneous coprecipitation of the precursors, assisted by ultrasound. This allows repetitive and high surface area values for calcined NiGa unsupported catalysts to be obtained. As has been studied,[32,38] the treatment at high temperatures in hydrogen atmosphere causes a decrease in the area value, being around 5 times lower than the calcined sample. Nevertheless, the values are still higher than those reported in the bibliography for Ni_5Ga_3 materials based on hydrotalcite.[36] Pore volume values around 0.3 $cm^3 \cdot g^{-1}$ were obtained, and the same trend as other authors has been observed,[34] detecting a decrease in pore volume with the increase in reduction temperature.

In Figure 1, the XRD diffractograms of fresh NiGa catalyst, calcined at 400 °C, and the samples reduced at 600, 700, and 800 °C are represented. For the fresh sample, signals at 37, 42.8, and 62.7° were observed and are characteristic of the cubic structure of the NiO phase (JCPDS 47-1049).[39] However, for the sample reduced at 600 °C, signals at 40.7 and 45.6° were detected and are related to the monoclinic $Ni_{13}Ga_9$ phase and lines at 31.9, 34.7, 35.9, 44.6, and 78.1°, which correspond to the metallic cubic Ni phase (JCPDS 04-0850), were also registered, together with a less-intense signal associated with trigonal Ni_2Ga_3 phase at 64.9°.[2,40,41] For the sample reduced at 700 °C, the signal characteristic of the cubic phase of NiGa at 65.7° appeared together with a significant increase in the Ni and $Ni_{13}Ga_9$ signals. When the NiGa catalyst was reduced at 800 °C, signals at 43 and 49° related to the orthorhombic phase of Ni_5Ga_3[36] could be observed, and a decrease in the signals of metallic Ni and $Ni_{13}Ga_9$ was also noticed.

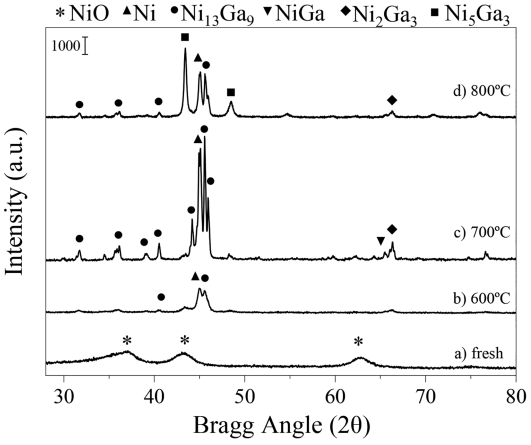

Figure 1. XRD patterns of (a) fresh NiGa catalyst and NiGa reduced at (b) 600 °C, (c) 700 °C, and (d) 800 °C.

The theoretical Ni/Ga ratio used in the synthesis was aimed to obtain δ-Ni_5Ga_3. At a calcination temperature of 400 °C in air, an amorphous NiO phase was obtained, and it was necessary to increase the temperature to achieve the Ni_5Ga_3 phase according to the phase equilibria diagram of the Ni-rich portion of the Ni−Ga binary system.[42] When the sample was treated in hydrogen at 600 °C, Ni^0 and the monoclinic intermetallic phase $Ni_{13}Ga_9$ were detected. By increasing the temperature to 700 °C, the intensity of the signals increased indicating a stabilization of the phases corresponding to Ni^0 and $Ni_{13}Ga_9$, the latter being a combination of Ni_5Ga_3 and NiGa, accompanied by the intermetallic phase that was segregated into cubic NiGa and trigonal Ni_2Ga_3. The treatment in a hydrogen flow at 800 °C produces Ni_5Ga_3, a Ni-rich phase that is described as the most suitable for the production of methanol.[43]

Raman spectra of the fresh and reduced NiGa samples were registered and are represented in Figure 2. The spectrum obtained for all the reduced samples (at 600, 700, and 800 °C) was similar and, for simplicity, only one of them is shown.

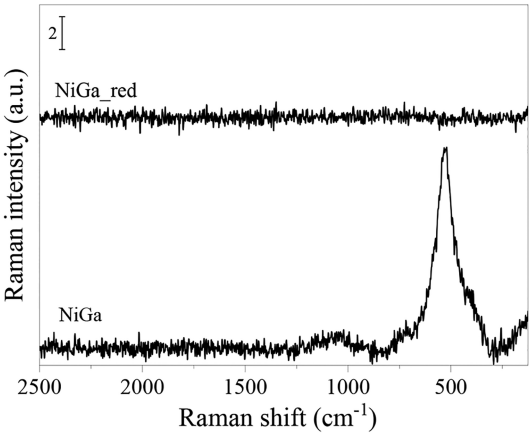

Figure 2. Raman spectra obtained for NiGa fresh catalyst and NiGa_red (reduced at any temperature).

The presence of an intense signal centered at 500 cm^{-1} and a weak band around 1090 cm^{-1} can be observed for the fresh catalyst (NiGa). Both signals correspond to the vibrational modes of nickel oxides,[44] in consonance with the amorphous band detected by XRD. On the other hand, signals related to β-Ga_2O_3[45] that should appear between 320 and 477 cm^{-1} were not detected. When the catalyst is reduced at temperatures between 600 and 800 °C, no signals were noticed. This could be explained by the disappearance of the NiO crystal structure in favor of the formation of other Ni phases, such as Ni^0, $Ni_{13}Ga_9$, or NiGa, as was confirmed by XRD, which are not Raman active species.

From the XPS data, the atomic surface composition was obtained, and the Ni/Ga ratio is represented in Table 2, together with the ratio between metallic and oxidized species for nickel and gallium, which were calculated through the deconvolution of Ni 2p and Ga $2p_{3/2}$ bands.

https://doi.org/10.1021/acs.iecr.1c03115
Ind. Eng. Chem. Res. 2021, 60, 18891−18899

Table 2. Ni/Ga, Ni^0/Ni^{2+}, and Ga^0/Ga^{3+} Ratios Obtained from XPS Data

	NiGa	NiGa_R600	NiGa_R700	NiGa_R800
Ni/Ga	2.03	1.08	1.23	1.52
Ni^0/Ni^{2+}	0	0.37	0.51	0.66
Ga^0/Ga^{3+}	0.46	1.18	1.29	1.57

Regarding the Ni/Ga ratio, which theoretically should have a value of 1.67 for the atomic ratio used in the preparative (Ni/Ga = 5/3), the values obtained were higher or lower depending on the temperature and the atmosphere of the treatment. For the sample calcined at 400 °C in air, the value was 2.03, indicating a superficial enrichment of Ni compared to the synthesis ratio, which should be related to the presence of NiO observed by XRD. Along the treatment in hydrogen, a variation from 1.08 to 1.52 was observed when the temperature increased from 600 to 800 °C, indicating that the structural modification provokes a variation of the Ni/Ga ratio and, in consequence, the surface species proportion changes. At 800 °C, the registered Ni/Ga value is the nearest to the initial theoretical ratio, which means that it would be close to the Ni_5Ga_3 structure, which is the main Ni_xGa_y phase detected by XRD.

Ni oxidation state was analyzed by Ni 2p signal and two nickel species were detected, with maxima at 851.4 eV (Ni^0) and 855.0 eV (Ni^{2+}).[41] The extent of reduction to metallic nickel was 0% after the calcination at 400 °C, but the hydrogen treatment at 600 °C produced an increase until 27%. The Ni^0/Ni^{2+} ratio almost linearly increased according to temperature of activation, with values of 0.51 and 0.66 for 700 and 800 °C, respectively. The reduction temperature with hydrogen causes the variation of the concentration of metallic nickel and consequently the bimetallic phases formed. It should be noted that the high content of Ni^0 and the Ni/Ga ratio would be intimately related to the route of the CO_2 hydrogenation process.

The gallium oxidation state was monitored by means of the Ga $2p_{3/2}$ signal and, for the fresh NiGa catalyst (calcined at 400 °C in air), it can be deconvolved into two bands, with maxima at 1116.1 and 1117.1 eV, which reveals the modification in the binding energy values and the presence of metallic Ga and Ga_2O_3,[46] respectively. The percentage of metallic Ga was 31% after the calcination at 400 °C and the activation in hydrogen at 600 °C increased this value until 54% as part of the intermetallic $Ni_{13}Ga_9$ species. This value remains practically constant with a slight increased up to 61% although the Ga^0/Ga^{3+} ratio increased from 1.18 to 1.57 when the temperature increased from 600 to 800 °C. Therefore, these facts suggest that gallium oxide two-dimensional nanoparticles should be highly dispersed on the surface, and they could disappear as the reduction temperature increases. These species together with Ni^0 are responsible for the Ni/Ga ratio obtained that was lower than the theoretical ratio for Ni_5Ga_3, which is the intermetallic unsupported phase suitable for methanol production.[37]

Additional TEM images with Ni and Ga atomic mapping are included as Supporting Information (Figure S1), and a uniform distribution of Ni and Ga species in aggregates was observed. When the activation temperature in the hydrogen atmosphere increased, the estimated average dimension of the aggregates varied from 20 to 50 nm. As was observed, XRD and XPS results for this high-surface-area unsupported material have evidenced structural changes in bulk and chemical changes in the surface when the catalyst is reduced at different temperatures for an initial Ni/Ga atomic ratio equal to 5/3. At 600 °C, there is a combination of metallic Ni and $Ni_{13}Ga_9$, with a Ni/Ga surface ratio of 1.08 with a maximum concentration of oxidized species (with the exception of NiGa calcined at 400 °C) of 73% Ni^{2+} and 46% Ga^{3+} related to the presence of very dispersed Ga_2O_3 which is only observable by XPS. At 700 °C, the proportion of Ni^0 and $Ni_{13}Ga_9$ intermetallic species increased, and the concentration of oxidized species decreased to 66 and 43% for Ni and Ga, respectively. When the activation temperature was 800 °C, the intermetallic species Ni_5Ga_3 is the main phase and the Ni/Ga surface ratio was 1.52, closer to the theoretical value.

3.2. Catalytic Activity. In this section, the reactivity results for the CO_2 hydrogenation reaction are presented for the unsupported catalyst that has undergone a H_2-treatment at different temperatures (600, 700, and 800 °C), evaluating the influence of the feeding ratio on the CO_2 thermoconversion. In Figure 3, the values of CO_2 conversion and CO selectivity are shown for the different H_2/CO_2 feed molar ratios using NiGa catalyst reduced at 600 °C. With this catalyst activated at 600 °C under these conditions, the only products detected were CO and CH_4. The CH_4 was the balance concentration, and its maximum estimated selectivity value was 3%; therefore, in consequence, only the CO selectivity values are represented. As can be seen (Figure 3a), for all stoichiometric H_2/CO_2 feed

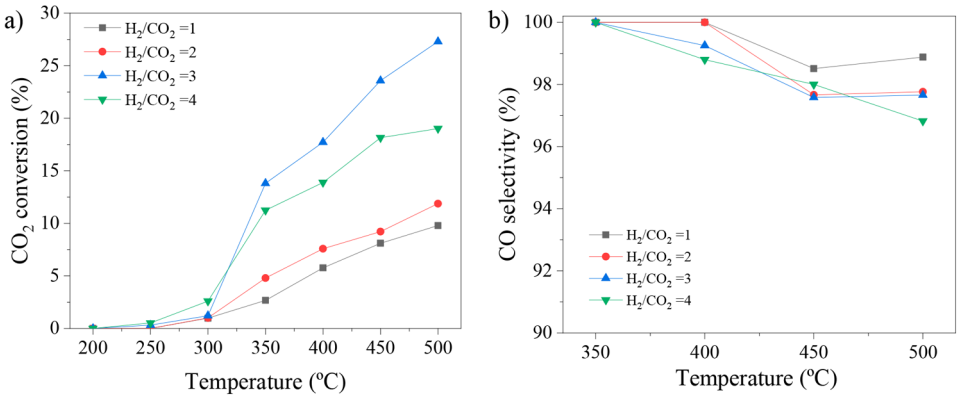

Figure 3. Influence of the inlet H_2/CO_2 ratio in (a) CO_2 conversion and (b) CO selectivity values according to reaction temperature for NiGa catalyst activated at 600 °C in H_2.

https://doi.org/10.1021/acs.iecr.1c03115
Ind. Eng. Chem. Res. 2021, 60, 18891−18899

ratios tested, the carbon dioxide conversion increases as the reaction temperature rises. For rWGS conditions (H_2/CO_2 = 1), there is an increase in conversion up to values of 9.8%. When the feed ratio is 2/1, the trend is parallel to the previous one and the maximum value registered is approximately 12%. For stoichiometric feeding conditions of methanol production (H_2/CO_2 = 3), a trend change is observed and the conversion values increase significantly. Up to 300 °C, the conversion values would practically coincide with those obtained for the lower ratios, but nevertheless, from 350 °C the conversion values tripled, reaching 27% at 500 °C, close to equilibrium (the comparison between experimental and equilibrium data are included in Figure S2).[47] For the feed ratio corresponding to methanation (H_2/CO_2 = 4), the conversion values are below the feed ratio for methanol production and above the stoichiometric values of rWGS. Although the curve has a sigmoidal trend and is similar to that obtained for feeding ratio 3, the maximum value reached is 19%.

In all cases and regardless of the feeding ratio, the formation of CO indicates that the predominant reaction is the reverse water gas shift reaction, and an increase in the reaction temperature causes in all cases a decrease in the selectivity to CO directed toward methane that is more significant for the H_2/CO_2 = 4 ratio, although the values are always higher than 97%.

The increase in conversion with respect to the reaction temperature is explained by the endothermic character of the rWGS reaction.[22] Gholami et al.,[48] who studied the hydrogenation of CO_2 using different H_2/CO_2 molar ratios from 2 to 5 using a Ni/Cr_2O_3 catalyst, reported a direct relationship between the feed molar ratio and CO_2 conversion, keeping the selectivity of the products stable. Nevertheless, for the intermetallic NiGa catalyst reduced at 600 °C, that conversion trend was only appreciable for H_2/CO_2 ratios ≤ 3. High levels of hydrogen, close to the stoichiometric levels of methanation, cause a decrease in CO_2 conversion due to the competitive chemisorption of the reagents. The surface would be saturated in hydrogen so that the interaction of CO_2 on the partially hydroxylated centers would decrease, decreasing the conversion of CO_2, although selectivity to CO is maintained. The population of surface sites should be active centers of the rWGS that involve reduced Ni sites since the mechanism would occur preferentially through the formation of carbonyls-like intermediates[49] as occurs with $Ni_{13}Ga_9$ phase, which is the formed phase, together with Ni^0, during the reduction with hydrogen at 600 °C. As suggested by XPS, 27% of Ni is reduced. The bulk structure is associated with the presence of $Ni_{13}Ga_9$ and the Ni/Ga atomic ratio is 1.08. These factors are responsible for the production of mainly CO with traces of CH_4 through rWGS reaction. As can be extracted, the selectivity of the CO product does not depend on the stoichiometric ratio of the feed.

In Figure 4, with the intention of analyzing how the treatment temperature governs the hydrogenation of CO_2 on this novel unsupported NiGa catalyst, the performance values obtained maintaining the H_2/CO_2 feed ratio at 3 are represented according to the reaction temperature. These operation conditions allow maximization of the CO_2-conversion and selectivity to the main direct products of CO_2 hydrogenation and correlate phases, surface species, and the most realistic reaction paths.

For the catalyst treated at 600 °C in hydrogen atmosphere, it can be observed that the yield of CO increases almost linearly

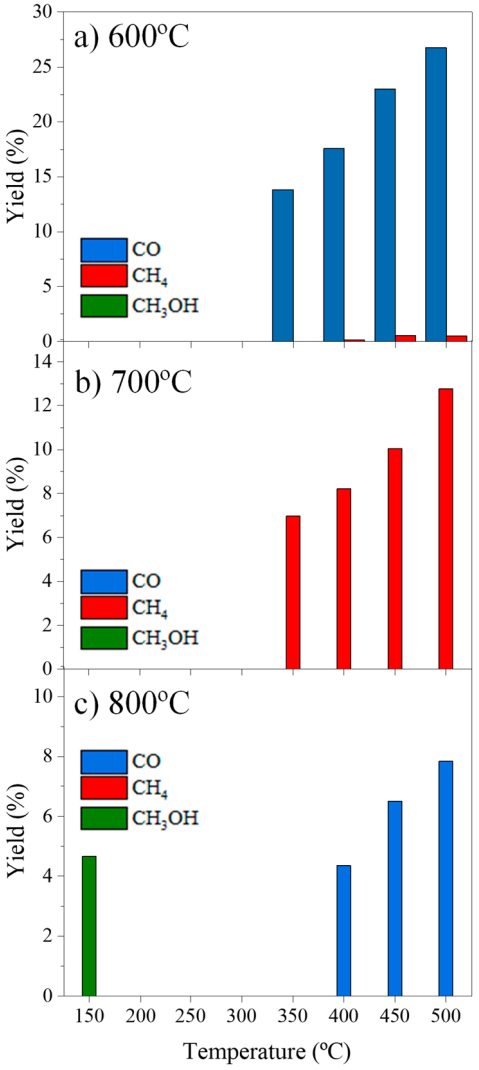

Figure 4. Yield of CO, CH_4, and CH_3OH according to reaction temperature for NiGa reduced at (a) 600, (b) 700, and (c) 800 °C using a H_2/CO_2 feed ratio of 3.

with the reaction temperature, and from 450 °C measurable amounts of methane are detected. It is important to note that when the catalyst is subjected to a temperature of 700 °C in hydrogen, CO or methanol are not observed at any temperature, being 100% selective to methane. The increase in the reaction temperature causes an almost exponential increase in methane yield values. The maximum conversion value reached is close to 13%. The modification of the treatment temperature to 800 °C in a hydrogen atmosphere in situ produces a radical modification in the CO_2 conversion profile. At 150 °C, the CO_2 conversion reaches 4.5%, and the selectivity is completely directed to methanol. When 400 °C is reached, under these conditions, the catalyst produce CO in a completely selective way. However, the performance values do not exceed 8% at the highest temperature.

When the Ni/Ga ratio is the lowest (1.08) the reverse water gas shift as an endothermic reaction prevails over CO_2-methanation with an observable increment of CO_2 conversion up to 27.3%. The experimental data collected at different temperatures for the catalyst treated at 700 °C show that regardless of the reaction temperature, the unique reaction is

https://doi.org/10.1021/acs.iecr.1c03115
Ind. Eng. Chem. Res. 2021, 60, 18891−18899

methanation, even when a lower than stoichiometric fraction of hydrogen is being fed, indicating that CO_2 activation is the key reaction step. These data suggest that the intermetallic phases present and the surface species distribution make the preponderant active sites differ from those observed for the catalyst treated at 600 °C, since the methane yield varies from 6.5 to 13% when the reaction temperature increases from 350 to 500 °C. A Ni metallic enriched surface was observed (surface atomic Ni/Ga = 1.23 and Ni^0/Ni^{2+} = 0.51) involving $Ni_{13}Ga_9$ and Ni^0 phases in a higher proportion. The accommodation of CO_2 on the surface would be an easier step on a more reduced surface,[32] as is the case for the catalyst activated at 700 °C favoring the methanation reaction.

According to Aziz et al,[50] the production of methane requires the combination of Ni sites for the dissociation of hydrogen and the presence of defect sites or oxygen vacancies for the formation of intermediate-carbon species. Therefore, another fundamental parameter that correlates phases and surface species for the thermochemical reduction of CO_2 is the oxygen environment for the different hydrogen-annealed catalysts. In Table 3, the O-type species contribution obtained from the deconvolution of the O 1s signal are shown. From the shape of the curve for the different treated materials, three kinds of oxygen species can be distinguished and, according to previous studies,[51,52] can be identified as O_I, O_{II}, and O_{III} oxygen-type species at binding energy values between 528−529 eV (lattice oxygen species, O^{2-}), lower than 530 eV (surface oxygen species, O_2^{2-} or O^-, O_2^-), and higher than 530 eV (oxygen from surface-chemisorbed groups, OH^-, CO_3^{2-}), respectively.

Table 3. O-Type Species Contribution (%) Obtained from the Deconvolution of O 1s Signal

	NiGa	NiGa_R600	NiGa_R700	NiGa_R800
O_I		9.7	15.4	10.8
O_{II}	72.1	15.7	39.2	36.3
O_{III}	27.9	74.6	45.4	52.9

For the calcined NiGa catalyst, the main contribution corresponded to the O_{II} species associated with surface oxides related to structural NiO and Ga_2O_3 phases. For the catalyst activated at 600 °C, the ratio between O_I and O_{II} with respect to O_{III} was 0.34, being the lowest estimated value. This ratio increased up to 1.20 with activation at 700 °C and decreased to 0.89 for the highest temperature of hydrogen treatment. Despite being an unsupported catalytic system as Ilsemann et al.[33] reported for the influence of the support on the methanation reaction, type O_I and O_{III} surface oxygen species can be here found where CO_2 is adsorbed in the form of carbonates and hydrogen carbonates. In addition, Ga_2O_3 can be carbonated during the reaction. In the same way, when oxygen vacancies are generated that are detected by XPS, there may be CO_2 activation on these sites.[53] Furthermore, there are metallic sites in which CO_2 can also interact. The multiphasic nickel−gallium catalyst reduced with hydrogen at 600 and 700 °C is able to produce CO and CH_4 from CO_2. The reactions likely possess some mechanistic commonalities. The reduction of CO_2 to CH_4 would involve the formation of carbonyl-like species bonded to the catalyst as a first step, being an intermediate of the process over Ni_xGa_y phases. For the surface developed species, which reflect the bulk composition, after in situ-700 °C hydrogen activation, there is a combination of O_I and O_{II} surface oxygen species and reduced Ni and $Ni_{13}Ga_9$ as main phases that makes the reaction completely selective to methane. The increase in reaction temperature also increased the CO_2 conversion due to the fact that the production of intermediate species is improved.[13] The surface Ni−Ga centers can be responsible for weakening the C−O bond through the strong interaction between surface oxygen species with CO molecules formed, which leads to the creation of a surface-carbon species and its further hydrogenation to methane. The methanation proceeds through an intermetallic NiGa, with a Ni metallic enriched phase, in which the interaction of carbon dioxide determines the CO_2-activation and hence the hydrogenation of CO_2 to CH_4.

Despite a hydrogen treatment of the catalyst at 800 °C, the sample is not completely reduced. Surface data reveal a combination of bimetallic and oxidized sites, with 48% of Ni^{2+} and 39% of Ga^{3+}, observing a transition of intermetallic species from $Ni_{13}Ga_9$ to Ni_5Ga_3, the latter being the main phase and related to a higher methanol production.[37] A discontinuity has been detected in the behavior of the catalyst as a function of the reaction temperature, probably associated with a change in the reaction pathway. The formation of methanol has been observed only at 150 °C with a CO_2 conversion of 4.5%, which is higher than values around 2−3% that are registered by other authors working at higher pressures.[36,37] When the reaction temperature exceeds 400 °C the selectivity of the process is complete to CO and the CO_2 conversion values reached 8%. The activity in terms of CO_2 conversion decreases as the activation temperature increases because there is an increase in the Ni/Ga ratio, and in agreement with the work of Gallo et al.,[43] the overall activity of CO_2 hydrogenation decreased with the Ni enrichment of the material surface. The characterization and reactivity results suggest that there exists a synergistic effect between Ga_2O_3 and intermetallic Ni_5Ga_3 for the methanol production from CO_2 reduction at atmospheric pressure. The presence of gallium oxide could improve the adsorption and activation of CO_2, which are also required for methanol formation. Therefore, the presence of Ni_5Ga_3 and Ga_2O_3 favors a higher number of active centers for the activation of CO_2. Since the process is at a low temperature and there is a highly hydrogenated surface, in these conditions formate-type species (HCOO*) should be promoted, although the formation would be limited by thermodynamic equilibrium. The formate species are subsequently hydrogenated to methanol in agreement with the work of Rasteiro et al.[37] Otherwise, the hydroxycarbonyl species (HO−*C═O)[35], which are highly reactive and precursors of the formation of rWGS products. could be formed by another reaction path. Since from 400 °C, the only product detected is CO, this is necessarily the route at high temperature.

Therefore, an understanding of the structural sensitivity and selectivity relationship considering the yield of CO, CH_4, and CH_3OH and the surface structural characteristics has been established, through a tentative pathway of CO_2 hydrogenation to rWGS, methanation, and methanol production, considering the most plausible key intermediates. As has been experimentally demonstrated, the mechanism of the reaction depends on the intrinsic nature of Ni_xGa_y intermetallic phases and the interaction between active Ni centers and the chemical environment promoted by the surrounding Ga atoms.

https://doi.org/10.1021/acs.iecr.1c03115
Ind. Eng. Chem. Res. 2021, 60, 18891−18899

4. CONCLUSIONS

An unsupported NiGa model catalyst with high surface area has been developed which, depending on the hydrogen treatment, allows the acquisition and tuning of main crystalline phases and surface species modifying CO_2 conversion and the selectivity of the CO_2 hydrogenation process to be directed preferentially to CO, CH_4, or CH_3OH formation. From the rational experimental design, the bulk and surface species have been identified and correlated with the catalytic activity and the preferential reaction pathway. After treatment in hydrogen at 600 °C, $Ni_{13}Ga_9$ and metallic Ni are the main phases, with a Ni/Ga surface ratio of 1.08, and the catalyst produces mainly CO, independently of the H_2/CO_2 feed ratio, via rWGS. At 700 °C, the increase in the proportion of Ni^0 and $Ni_{13}Ga_9$, together with the species of surface oxygen, O_I and O_{II}, direct the hydrogenation reaction of CO_2 to methane. At 800 °C, Ni_5Ga_3 is the main phase detected and methanol is produced at low temperature, via formate as intermediate, and above 400 °C, the CO-selectivity is complete, through the rWGS reaction.

■ ASSOCIATED CONTENT

Supporting Information

The Supporting Information is available free of charge at https://pubs.acs.org/doi/10.1021/acs.iecr.1c03115.

Ni and Ga mapping images registered in TEM Talos F200X for NiGa catalyst activated in hydrogen at 600, 700, and 800 °C; Comparison of experimental and equilibrium CO_2 conversion obtained at 500 °C and at different H_2/CO_2 ratio represented with the inlet CO_2 molar fraction (PDF)

■ AUTHOR INFORMATION

Corresponding Author

Luis J. Alemany − *Departamento de Ingeniería Química, Facultad de Ciencias, Universidad de Málaga, Málaga E-29071, Spain;* orcid.org/0000-0002-7428-4718; Phone: +34952131919; Email: luijo@uma.es

Authors

Marina Cortés-Reyes − *Departamento de Ingeniería Química, Facultad de Ciencias, Universidad de Málaga, Málaga E-29071, Spain;* orcid.org/0000-0002-7314-3673

Ibrahim Azaoum − *Departamento de Ingeniería Química, Facultad de Ciencias, Universidad de Málaga, Málaga E-29071, Spain*

Sergio Molina-Ramírez − *Departamento de Ingeniería Química, Facultad de Ciencias, Universidad de Málaga, Málaga E-29071, Spain*

Concepción Herrera − *Departamento de Ingeniería Química, Facultad de Ciencias, Universidad de Málaga, Málaga E-29071, Spain*

M. Ángeles Larrubia − *Departamento de Ingeniería Química, Facultad de Ciencias, Universidad de Málaga, Málaga E-29071, Spain*

Complete contact information is available at: https://pubs.acs.org/10.1021/acs.iecr.1c03115

Notes

The authors declare no competing financial interest.

■ ACKNOWLEDGMENTS

The research group PROCAT from the University of Malaga, Spain, is grateful for the invitation to participate in this Special Issue in recognition and tribute to Professor José Luis García Fierro of Institute of Catalysis and Petrochemistry, CSIC (Spain), and also wishes to express a deep appreciation to Professor J.L.G. Fierro.

■ ABBREVIATIONS

XRD = X-ray diffraction
BET = Brunauer−Emmett−Teller
TEM = transmission electron microscopy
XPS = X-ray photoelectron spectroscopy

■ REFERENCES

(1) Gao, Y.; Gao, X.; Zhang, X. The 2 °C Global Temperature Target and the Evolution of the Long-Term Goal of Addressing Climate Change—From the United Nations Framework Convention on Climate Change to the Paris Agreement. *Engineering* **2017**, *3* (2), 272−278.

(2) Molina-Ramírez, S.; Cortés-Reyes, M.; Herrera, C.; Larrubia, M. A.; Alemany, L. J. CO_2-SR Cyclic Technology: CO_2 Storage and in Situ Regeneration with CH_4 over a New Dual Function NiBa Unsupported Catalyst. *J. CO2 Util.* **2020**, *40*, 101201.

(3) Benhelal, E.; Shamsaei, E.; Rashid, M. I. Challenges against CO_2 Abatement Strategies in Cement Industry: A Review. *J. Environ. Sci.* **2021**, *104*, 84−101.

(4) Oliveira, T.; Varum, C.; Botelho, A. Econometric Modeling of CO_2 Emissions Abatement: Comparing Alternative Approaches. *Renewable Sustainable Energy Rev.* **2019**, *105*, 310−322.

(5) Asghar, U.; Rafiq, S.; Anwar, A.; Iqbal, T.; Ahmed, A.; Jamil, F.; Khurram, M. S.; Akbar, M. M.; Farooq, A.; Shah, N. S.; Park, Y.-K. Review on the Progress in Emission Control Technologies for the Abatement of CO_2, SOx and NOx from Fuel Combustion. *J. Environ. Chem. Eng.* **2021**, *9*, 106064.

(6) Murena, F.; Esposito, S.; Deorsola, F. A.; Galletti, C.; Prati, M. V. CO_2 Abatement and CH4 Recovery at Vehicle Exhausts: Comparison and Characterization of Ru Powder and Pellet Catalysts. *Int. J. Hydrogen Energy* **2020**, *45* (15), 8640−8648.

(7) Svensson, R.; Odenberger, M.; Johnsson, F.; Strömberg, L. Transportation Systems for CO_2 - Application to Carbon Capture and Storage. *Energy Convers. Manage.* **2004**, *45* (15−16), 2343−2353.

(8) Wang, M.; Lawal, A.; Stephenson, P.; Sidders, J.; Ramshaw, C. Post-Combustion CO_2 Capture with Chemical Absorption: A State-of-the-Art Review. *Chem. Eng. Res. Des.* **2011**, *89* (9), 1609−1624.

(9) Zhou, Y.; Huang, Y.; Jin, B.; Luo, X.; Liang, Z. Pd Nanoclusters-Based Catalysts with Schiff Base Modifying Carrier for CO_2 Hydrogenation to Formic Acid. *Ind. Eng. Chem. Res.* **2019**, *58*, 44−52.

(10) Montzka, S. A.; Dlugokencky, E. J.; Butler, J. H. Non-CO_2 Greenhouse Gases and Climate Change. *Nature* **2011**, *476* (7358), 43−50.

(11) Schaaf, T.; Grünig, J.; Schuster, M. R.; Rothenfluh, T.; Orth, A. Methanation of CO_2 - Storage of Renewable Energy in a Gas Distribution System. *Energy. Sustain. Soc.* **2014**, *4*, 1−14.

(12) An, X.; Zuo, Y.-Z.; Zhang, Q.; Wang, D.-Z.; Wang, J.-F. Dimethyl Ether Synthesis from CO_2 Hydrogenation on a CuO-ZnO-Al_2O_3-ZrO_2/HZSM-5 Bifunctional Catalyst. *Ind. Eng. Chem. Res.* **2008**, *47*, 6547−6554.

(13) Yu, Y.; Bian, Z.; Wang, J.; Wang, Z.; Tan, W.; Zhong, Q.; Kawi, S. CO_2 Hydrogenation to CH_4 over Hydrothermal Prepared Ceria-Nickel Catalysts: Performance and Mechanism Study. *Catal. Today* **2021**, 1−9.

(14) Gutterød, E. S.; Øien-ØDegaard, S.; Bossers, K.; Nieuwelink, A.-E.; Manzoli, M.; Braglia, L.; Lazzarini, A.; Borfecchia, E.; Ahmadigoltapeh, S.; Bouchevreau, B.; Lønstad-Bleken, B. T.; Henry, R.; Lamberti, C.; Bordiga, S.; Weckhuysen, B. M.; Lillerud, K. P.;

Olsbye, U. CO_2 Hydrogenation over Pt-Containing UiO-67 Zr-MOFs - The Basecase. *Ind. Eng. Chem. Res.* **2017**, *56*, 13206−13218.
(15) Saeidi, S.; Najari, S.; Fazlollahi, F.; Nikoo, M. K.; Sefidkon, F.; Klemeš, J. J.; Baxter, L. L. Mechanisms and Kinetics of CO_2 Hydrogenation to Value-Added Products: A Detailed Review on Current Status and Future Trends. *Renewable Sustainable Energy Rev.* **2017**, *80*, 1292−1311.
(16) Herrera, C.; Cortés-Reyes, M.; Larrubia, M. Á.; Domínguez-Barroso, M. V.; Díaz-Rey, M. R.; Alemany, L. J. Dimethyl Ether Synthesis via Methanol Dehydration over Ta-Supported Catalysts. *Appl. Catal., A* **2019**, *582*, 117088.
(17) Pinilla-Herrero, I.; Olsbye, U.; Márquez-Álvarez, C.; Sastre, E. Effect of Framework Topology of SAPO Catalysts on Selectivity and Deactivation Profile in the Methanol-to-Olefins Reaction. *J. Catal.* **2017**, *352*, 191−207.
(18) Ren, S.; Fan, X.; Shang, Z.; Shoemaker, W. R.; Ma, L.; Wu, T.; Li, S.; Klinghoffer, N. B.; Yu, M.; Liang, X. Enhanced Catalytic Performance of Zr Modified CuO/ZnO/Al_2O_3 Catalyst for Methanol and DME Synthesis via CO_2 Hydrogenation. *J. CO2 Util.* **2020**, *36*, 82−95.
(19) Wang, W.; Jiang, X.; Wang, X.; Song, C. Fe-Cu Bimetallic Catalysts for Selective CO_2 Hydrogenation to Olefin-Rich C2+ Hydrocarbons. *Ind. Eng. Chem. Res.* **2018**, *57*, 4535−4542.
(20) Stangeland, K.; Li, H.; Yu, Z. Thermodynamic Analysis of Chemical and Phase Equilibria in CO_2 Hydrogenation to Methanol, Dimethyl Ether, and Higher Alcohols. *Ind. Eng. Chem. Res.* **2018**, *57*, 4081−4094.
(21) Hu, M.; He, J.; Guo, R.; Yuan, W.; Xi, W.; Luo, J.; Ding, Y. Visualizing Oxidation of Cu Nanoparticles at Atomic Resolution during the Reverse Water-Gas Shift Reaction. *Catal. Commun.* **2020**, *146*, 106129.
(22) Jurković, D. L.; Pohar, A.; Dasireddy, V. D. B. C.; Likozar, B. Effect of Copper-Based Catalyst Support on Reverse Water-Gas Shift Reaction (RWGS) Activity for CO_2 Reduction. *Chem. Eng. Technol.* **2017**, *40* (5), 973−980.
(23) Goguet, A.; Meunier, F. C.; Tibiletti, D.; Breen, J. P.; Burch, R. Spectrokinetic Investigation of Reverse Water-Gas-Shift Reaction Intermediates over a Pt/CeO_2 Catalyst. *J. Phys. Chem. B* **2004**, *108*, 20240−20246.
(24) Gao, J.; Song, F.; Li, Y.; Cheng, W.; Yuan, H.; Xu, Q. Cu_2In Nanoalloy Enhanced Performance of Cu/ZrO_2 Catalysts for the CO_2 Hydrogenation to Methanol. *Ind. Eng. Chem. Res.* **2020**, *59*, 12331−12337.
(25) Wang, Y.; Wu, D.; Liu, T.; Liu, G.; Hong, X. Fabrication of PdZn Alloy Catalysts Supported on ZnFe Composite Oxide for CO_2 Hydrogenation to Methanol. *J. Colloid Interface Sci.* **2021**, *597*, 260−268.
(26) Liang, B.; Ma, J.; Su, X.; Yang, C.; Duan, H.; Zhou, H.; Deng, S.; Li, L.; Huang, Y. Investigation on Deactivation of Cu/ZnO/Al_2O_3 Catalyst for CO_2 Hydrogenation to Methanol. *Ind. Eng. Chem. Res.* **2019**, *58*, 9030−9037.
(27) Chang, K.; Wang, T.; Chen, J. G. Methanol Synthesis from CO_2 Hydrogenation over CuZnCeTi Mixed Oxide Catalysts. *Ind. Eng. Chem. Res.* **2019**, *58*, 7922−7928.
(28) Fang, T.; Liu, B.; Lian, Y.; Zhang, Z. Selective Methanol Synthesis from CO_2 Hydrogenation over an In_2O_3/Co/C-N Catalyst. *Ind. Eng. Chem. Res.* **2020**, *59*, 19162−19167.
(29) Díez-Ramírez, J.; Díaz, J. A.; Dorado, F.; Sánchez, P. Kinetics of the Hydrogenation of CO_2 to Methanol at Atmospheric Pressure Using a Pd-Cu-Zn/SiC Catalyst. *Fuel Process. Technol.* **2018**, *173*, 173−181.
(30) Studt, F.; Sharafutdinov, I.; Abild-Pedersen, F.; Elkjær, C. F.; Hummelshøj, J. S.; Dahl, S.; Chorkendorff, I.; Nørskov, J. K. Discovery of a Ni-Ga Catalyst for Carbon Dioxide Reduction to Methanol. *Nat. Chem.* **2014**, *6*, 320−324.
(31) Jacquemin, M.; Beuls, A.; Ruiz, P. Catalytic Production of Methane from CO_2 and H_2 at Low Temperature: Insight on the Reaction Mechanism. *Catal. Today* **2010**, *157*, 462−466.
(32) Liu, H.; Xu, S.; Zhou, G.; Huang, G.; Huang, S.; Xiong, K. CO_2 Hydrogenation to Methane over Co/KIT-6 Catalyst: Effect of Reduction Temperature. *Chem. Eng. J.* **2018**, *351*, 65−73.
(33) Ilsemann, J.; Murshed, M. M.; Gesing, T. M.; Kopyscinski, J.; Bäumer, M. On the Support Dependency of the CO_2 Methanation − Decoupling Size and Support Effects. *Catal. Sci. Technol.* **2021**, *11*, 4098−4114.
(34) Navarro, J. C.; Centeno, M. A.; Laguna, O. H.; Odriozola, J. A. Ru−Ni/$MgAl_2O_4$ Structured Catalyst for CO_2 Methanation. *Renewable Energy* **2020**, *161*, 120−132.
(35) Gong, J.; Chu, M.; Guan, W.; Liu, Y.; Zhong, Q.; Cao, M.; Xu, Y. Regulating the Interfacial Synergy of Ni/Ga_2O_3 for CO_2 Hydrogenation toward the Reverse Water-Gas Shift Reaction. *Ind. Eng. Chem. Res.* **2021**, *60*, 9448.
(36) Men, Y.; Fang, X.; Gu, Q.; Singh, R.; Wu, F.; Danaci, D.; Zhao, Q.; Xiao, P.; Webley, P. A. Synthesis of Ni_5Ga_3 Catalyst by Hydrotalcite-like Compound (HTlc) Precursors for CO_2 Hydrogenation to Methanol. *Appl. Catal., B* **2020**, *275*, 119067.
(37) Rasteiro, L. F.; Rossi, M. A. L. S.; Assaf, J. M.; Assaf, E. M. Low-Pressure Hydrogenation of CO_2 to Methanol over Ni-Ga Alloys Synthesized by a Surfactant-Assisted Co-Precipitation Method and a Proposed Mechanism by DRIFTS Analysis. *Catal. Today* **2021**, *381*, 261−271.
(38) Li, K.; Wang, H.; Wei, Y.; Yan, D. Transformation of Methane into Synthesis Gas Using the Redox Property of Ce-Fe Mixed Oxides: Effect of Calcination Temperature. *Int. J. Hydrogen Energy* **2011**, *36*, 3471−3482.
(39) Zhang, R.; Shi, J.; Zhou, T.; Tu, J.; Zhang, T. A Yolk-Double-Shelled Heterostructure-Based Sensor for Acetone Detecting Application. *J. Colloid Interface Sci.* **2019**, *539*, 490−496.
(40) He, S.; Pfau, A. J.; Diulus, J. T.; Albuquerque, G. H.; Herman, G. S. Deposition and Characterization of Nickel Gallium Thin Films. *J. Vac. Sci. Technol., A* **2018**, *36* (3), 031402.
(41) García-Diéguez, M.; Pieta, I. S.; Herrera, M. C.; Larrubia, M. A.; Alemany, L. J. Nanostructured Pt- and Ni-Based Catalysts for CO_2-Reforming of Methane. *J. Catal.* **2010**, *270*, 136−145.
(42) Ducher, R.; Kainuma, R.; Ishida, K. Phase Equilibria in the Ni-Rich Portion of the Ni-Ga Binary System. *Intermetallics* **2007**, *15*, 148−153.
(43) Gallo, A.; Snider, J. L.; Sokaras, D.; Nordlund, D.; Kroll, T.; Ogasawara, H.; Kovarik, L.; Duyar, M. S.; Jaramillo, T. F. Ni_5Ga_3 Catalysts for CO_2 Reduction to Methanol: Exploring the Role of Ga Surface Oxidation/Reduction on Catalytic Activity. *Appl. Catal., B* **2020**, *267*, 118369.
(44) Faid, A. Y.; Barnett, A. O.; Seland, F.; Sunde, S. Ni/NiO Nanosheets for Alkaline Hydrogen Evolution Reaction: In Situ Electrochemical-Raman Study. *Electrochim. Acta* **2020**, *361*, 137040.
(45) Zhong, M.; Wei, Z.; Meng, X.; Wu, F.; Li, J. High-Performance Single Crystalline UV Photodetectors of β-Ga_2O_3. *J. Alloys Compd.* **2015**, *619*, 572−575.
(46) Moulder, J. F.; Stickle, W. F.; Sobol, P. E.; Bomben, K. D. *Handbook of X-Ray Photoelectron Spectroscopy*; Perkin-Elmer Co., 1992.
(47) Lim, H. S.; Lee, M.; Kim, Y.; Kang, D.; Lee, J. W. Low-Temperature CO_2 Hydrogenation to CO on Ni-Incorporated $LaCoO_3$ Perovskite Catalysts. *Int. J. Hydrogen Energy* **2021**, *46*, 15497−15506.
(48) Gholami, S.; Alavi, S. M.; Rezaei, M. Synthesis of Cr_2O_3-Al_2O_3 Powders with Various Cr_2O_3/Al_2O_3 Molar Ratios and Their Applications as Support for the Preparation of Nickel Catalysts in CO_2 Methanation Reaction. *Int. J. Hydrogen Energy* **2021**, *46*, 5311−5322.
(49) Bobadilla, L. F.; Santos, J. L.; Ivanova, S.; Odriozola, J. A.; Urakawa, A. Unravelling the Role of Oxygen Vacancies in the Mechanism of the Reverse Water-Gas Shift Reaction by Operando DRIFTS and Ultraviolet-Visible Spectroscopy. *ACS Catal.* **2018**, *8* (8), 7455−7467.
(50) Aziz, M. A. A.; Jalil, A. A.; Triwahyono, S.; Mukti, R. R.; Taufiq-Yap, Y. H.; Sazegar, M. R. Highly Active Ni-Promoted Mesostruc-

https://doi.org/10.1021/acs.iecr.1c03115
Ind. Eng. Chem. Res. 2021, 60, 18891−18899

tured Silica Nanoparticles for CO_2 Methanation. *Appl. Catal., B* **2014**, *147*, 359−368.
(51) Cortés-Reyes, M.; Martínez-Munuera, J. C.; Herrera, C.; Larrubia, M. Á.; Alemany, L. J.; García-García, A. Isotopic Study of the Influence of Oxygen Interaction and Surface Species over Different Catalysts on the Soot Removal Mechanism. *Catal. Today* **2021**, DOI: 10.1016/j.cattod.2021.07.015.
(52) Zhao, K.; Shen, Y.; Huang, Z.; He, F.; Wei, G.; Zheng, A.; Li, H.; Zhao, Z. Different Oxidation Routes for Lattice Oxygen Recovery of Double-Perovskite Type Oxides $LaSrFeCoO_6$ as Oxygen Carriers for Chemical Looping Steam Methane Reforming. *J. Energy Chem.* **2017**, *26*, 501−509.
(53) Tan, Q.; Shi, Z.; Wu, D. CO_2 Hydrogenation to Methanol over a Highly Active Cu-Ni/CeO_2-Nanotube Catalyst. *Ind. Eng. Chem. Res.* **2018**, *57*, 10148−10158.

https://doi.org/10.1021/acs.iecr.1c03115
Ind. Eng. Chem. Res. 2021, 60, 18891−18899